Araştırma Makalesi / *Research Article*
Fizik / *Physics*

Iğdır Üniversitesi Fen Bilimleri Enstitüsü Dergisi, 10(1): 202-213, 2020
***Journal of the Institute of Science and Technology,* 10(1): 202-213, 2020**

DOI: 10.21597/jist.640027

ISSN: 2146-0574, eISSN: 2536-4618

Determination of Radiation Protection Features of the Ag_2O Doped Boro-Tellurite Glasses Using Phy-X / PSD Software

Bünyamin ALIM[1]*

ABSTRACT: This study focused on the radiation protection features of the Ag_2O doped boro-tellurite glass samples in the form of $(x)Ag_2O/(100-x)(65B_2O_3\text{-}35TeO_2)$ where x=10, 15, 20, 25 and 30 mol%. by using Phy-X / PSD software, the radiation protection parameters such as mass attenuation coefficient (MAC), linear attenuation coefficient (LAC), half-value layer (HVL), mean free path (MFP), total atomic and electronic cross-sections (ACS and ECS), effective atomic number (Z_{eff}) , effective electron density (N_{eff}) and effective conductivity (σ_{eff}) of present glasses were calculated in the photon energy range of 0.015-15 MeV. In order to evaluation the usability of these glasses in terms of radiation protection, the all investigated protection parameters were also calculated for commercial RS 253 glass and some concretes such as ordinary concrete (OC), hematite-serpenite (HS) and basalt-magnetite (BM) that are commonly used as shielding material in the nuclear application. The results obtained were evaluated in terms of both photon energy and chemical composition of the glasses examined. Additionally, the results obtained for the examined glasses were compared with the corresponding values obtained for the comparison materials presented to determine the best radiation protection glass. It was clearly observed that the MAC, LAC, ACS, ECS and Z_{eff} values increased with the increasing of molar doping percentage Ag_2O in the glasses. It was found that the radiation protection capacities of the Ag_2O doped boro-tellurite glasses is found higher than the other compared materials. Maximum MAC, LAC, ACS, ECS and Z_{eff} values were observed in the sample of G5 that contains 30% Ag_2O. This study indicates that the disilver oxide doped tellurite glasses can be developed as radiation protection materials for many nuclear applications.

Keywords: Mass attenuation coefficient, radiation shielding, tellurite glasses, effective atomic number, effective conductivity.

[1] Bünyamin ALIM (**Orcid ID:** 0000-0002-4143-9787), Technical Scientific Vocational School, Department of Electricity and Energy, Bayburt University, Bayburt, Turkey

*Sorumlu Yazar/Corresponding Author: Bünyamin ALIM, e-mail: balim@bayburt.edu.tr

Geliş tarihi / *Received:* 30-10-2019
Kabul tarihi / *Accepted:* 28-11-2019

INTRODUCTION

X- and gamma rays are used in many fields such as imaging systems, material characterization processes and medical treatment because of their high penetration properties. However, if these high-energy rays affect living organs, they can cause permanent damage to living tissues. Therefore, the interaction of unwanted amounts of radiation with living organisms should be minimized. The need for radiation-shielding materials having the desired properties to protect living tissues from the harmful effects of radiation is evident. Although lead (Pb) is the most widely used element in radiation protection, there are several limitations in its use due to its low melting point and high toxic effects. Therefore, researchers are investigating different alternative materials such as glass (Sayyed and Elhouichet 2017; Ersundu et al., 2018), concrete (Aygün et al., 2019), polymer (Kaçal et al., 2019; Abdalsalam et al., 2019), ceramics (Akman et al., 2019), alloy (Han and Demir, 2009; Han and Demir, 2010; Han et al., 2012; Akman et al., 2019; Şakar et al., 2019; Agar et al., 2019; Alım et al., 2020a,b) and star dust (Han et al., 2015) that have some superior properties to improve radiation safety. The most important of these superior properties are high corrosion resistance, high density, non-toxicity and transparency. Therefore, recently, glasses have become the point of interest of researchers due to aforementioned their superior properties and they have developed glasses with different compositions as radiation shielding materials.

Telluride based glasses have unique properties which make them useful for a numerous of technical applications such as thermal imaging, optical data storage, lasers, optoelectronic devices. Due to their low crystallization ability (Shioya et al., 1995), high dielectric constant (Ahmad et al., 2006), low glass transition and melting temperature (Stanworth, 1952), high thermal stability and chemical resistance (El-Mallawany 2016), these glasses are frequently used in recent research. In spite of wide range applications, it is well known that, tellurium oxide (TeO_2) does not turn into a glassy form without the addition of a secondary ingredient under traditional quenching rates (Övençoğlu et al., 2006). Therefore, alkali metal oxides (Xu et al., 2013), alkaline earth metal (Desirena 2009), heavy metal oxides (HMO) (Ersundu et al., 2018) and halogens (El-Mallawany, 1992) can be used as network modifiers to obtain tellurite-based glasses. A great number of studies have been reported in the literature on investigation of optical, thermal and structural properties of these glasses as a function of other participating materials (Lambson et al., 1984; El-Mallawany and Sounders, 1988; El-Mallawany et al., 1994; Sidkey et al., 1997; Rajendran et al., 2003).

In order to obtain telluride-based glasses, one of the most commonly used materials as a network modifier is B_2O_3. This binary structure is called as boro-telluride glasses. This glass system represents suitable for the necessity of thermal stability, low phonon energy, good transparency and chemical resistance (Sayyed and Elhouichet 2017). Moreover, disilver oxide (Ag_2O) can be used as glass former. Hallimah et al. (2005) reported that, the addition of Ag_2O as a third component to the borotelluride glasses, the molar volume and density increased by filling interstitial sites in the network by Ag^+ ions.
In literature, there are some studying in terms of radiation shielding properties of boro telluride glasses that are modified by zinc molybdenum and titanate bismuth (Lakshminarayana et al. 2017, 2018). The effect of doping of Ag_2O compound on the radiation protection capabilities of boro telluride glasses was first investigated in this study and it was aimed to investigate the radiation protection features of these glasses. For this purpose, $(x)Ag_2O/(100-x)(65B_2O_5\text{-}35TeO_2)$, where x=10, 15, 20, 25 and 30 mol% glasses, were selected for the investigations and the densities of the glasses were taken from a study reported by El-Moneim (El-Moneim, 2009) in advance. The calculated results were compared with commercial shielding glass and some concretes (ordinary concrete (OC), hematite-serpenite (HS) and

basalt-magnetite (BM)) (Bashter, 1997) to be able to make a significant evaluation about the photon shielding performances of the examined glasses.

MATERIALS AND METHODS

In transmission calculations without scattering effects, the number of photons coming to the target material exponentially attenuate depending on the thickness, density and absorption capacity of the composite. The relationship between the intensities of un-attenuated (I_0) and attenuated (I) photons in this is explained by the Beer-Lambert law:

$$I = I_0 e^{-\mu t} \tag{1}$$

where, t (cm) and μ (cm^{-1}) are the thickness and linear attenuation coefficient (LAC) of the absorber material, respectively. Although the LAC parameter provides leading information for photon-substance interactions, it does not provide information about the full absorption ability of a material. Therefore, in order to make a determination of the photon shielding capacity of absorber based on the material characteristic, the mass attenuation coefficient (MAC) obtained by dividing the LAC value by the density (ρ; gcm^{-3}) of the material is used and this parameter is calculated as follows:

$$\mu_m = \frac{\mu}{\rho} \tag{2}$$

In any composite material consisting of more than one element, a total MAC value for the entire material can be calculated using the Eq. 3:

$$\mu_m = (\mu/\rho) = \sum_i w_i (\mu/\rho)_i \tag{3}$$

where, w_i is the fractional weight of the i^{th} constituent element.

In some applications, the thickness information necessary to halve the number of photons coming to any material is required, and this thickness value is defined as the half-value layer (HVL). Mean free path (MFP) is the mean distance a photon travels between consecutive interactions. The HVL and MFP parameters can be calculated using LAC value of the samples and given as following expressions:

$$HVL = \frac{\ln(2)}{\mu} \tag{4}$$

$$MFP = \frac{1}{\mu} \tag{5}$$

The probability of mono-energetic photons coming on the material at any energy value to interact with the atoms and electrons in this material is defined as total atomic and electronic cross-sections (ACS (σ_T) and ECS (σ_e)), respectively. Both parameters have the unit cm^2g^{-1} (or barns/atom) and are calculated using Eqs. 6 and 7:

$$ACS = \sigma_T = \frac{\sum_i f_i A_i}{N_A} \mu_m \tag{6}$$

$$ECS = \sigma_e = \left(\frac{1}{N_A}\right) \sum_i \left(\frac{f_i A_i}{Z_i} (\mu_m)_i\right) \tag{7}$$

In these equations, N_A is the Avogadro number and f_i, A_i and Z_i are the mol fraction, atomic weight and atomic number of the i^{th} constituent element in the material.

The virtual atomic and electron number that defines a complex material consisting of more than one element in terms of photon shielding depending on the incoming radiation energy are called as the

effective atomic number (Z_{eff}) and effective electron density (N_{eff}). Since the elements that have high atomic numbers shows superior radiation shielding properties, the materials with high Z_{eff} value considered as good radiation absorber. The Z_{eff} can be calculated as follow:

$$Z_{eff} = \frac{\sigma_T}{\sigma_e} \tag{8}$$

Energy-dependent effective electron density is also calculated as follows:

$$N_{eff} = \frac{N_A}{\sum_i f_i A_i} Z_{eff} \sum n_i = \frac{\mu_m}{\sigma_e} \tag{9}$$

where, $\sum n_i$ is the total number of elements in the investigated material.

The effective conductivity (σ_{eff}) values of any material can be calculated as follows:

$$\sigma_{eff} = \left(\frac{N_{eff} \rho e^2 \tau}{m_e} \right) 10^3 \tag{10}$$

where m_e (kg) and e (Coulomb) are the mass and charge of electron, respectively. N_{eff} should be considered in the unit of electrons kg^{-1}. τ (s) is relaxation time of the electron at the Fermi Surface and is calculated using the following equation:

$$\tau = \frac{\hbar}{k_B T} = \frac{h}{2\pi k_B T} \tag{11}$$

where $T(K)$, $k_B(JK^{-1})$ and $h(J.s)$ are the ambient temperature of the material, Boltzman constant and Planck constant, respectively. The more detailed information about the parameters examined in this study was reported in our previous article (Alım et al., 2020a).

In this study, all calculations were done by using WinXCOM (Gerward et al., 2004) based Phy-X / PSD (Şakar et al., 2020) software.

RESULTS AND DISCUSSION

The boro-telluride glasses examined in this study were coded as G1, G2, G3, G4 and G5, respectively, with respect to the increasing molar percentage of Ag_2O compound that are doped to glasses. The chemical formulas, average molecular weight (AMW) and densities of the Ag_2O doped boro-telluride ternary system glasses under examination and weight fractions of constituent element in these glasses are given in Table 1. The mass attenuation coefficients (MACs) of the all samples under examination have been computed with WinXCOM based Phy-X/PSD software in the photon energy range between 0.015 and 15 MeV. The MAC values of the all present samples in the photon energy range of 0.015-15 MeV are given in Table 2. The variations of the MAC values versus the incident photon energies are shown in Fig. 1(a). As can be clearly seen from this figure, the MAC values change with the changes of primary photon energies and chemical compositions of the material investigated. In the low energy region (0.015-0.5 MeV), MAC values decrease sharply with the increasing photon energy. It is due to the dominance of the photoelectric absorption in this energy region. It is well known that the absorption cross-section of the photoelectric effect changes with atomic number of the material as Z^{4-5} and energy of the primary photon as $E^{-3.5}$. For this reason, it was found that MAC values of the glasses investigated and compared materials have highest in the low energy region. In the energy range of 0.015-0.5 MeV, it was observed that the highest MAC values were in the G5 sample (30% Ag_2O) and the lowest MAC values were in the OC sample. Furthermore, it was clearly seen that, with the increasing the molar percentage of Ag_2O compound in the boro-tellurite glasses, the MAC values increase. The

decreasing order of MAC values of the present samples at the same energy was obtained as G5> G4> G3> G2> G1> HS> BM> RS 253> OC. This shows that Ag_2O doped glasses have better absorption capacity than other comparative materials. Furthermore, it can be seen that the MAC values of glasses under examination have a sudden increase in the value of 0.025 MeV energy. This sudden increase is due to the K-shell absorption edge of the Ag element doped to telluride glasses. In parallel with increasing energy, the MAC values of all the materials examined have almost the same values in the energy range of about 0.5-3.38 MeV. Because Compton scattering is dominant in this energy range, MAC values are almost independent of the chemical composition of the investigated material. In the high-energy range following Compton scattering region, the Pair production (threshold value = 1.02 MeV) process starts and the MAC values are proportional to Z. Because the absorption probability is minimal in the region where Compton scattering is dominant, a relative increase is seen with increasing energy in MAC values in the pair production region with respect to Compton scattering region.

Table 1. Chemical compositions, densities of the Ag_2O doped boro-tellurite glasses and weight fractions of constituent element in these glasses.

				Weight Fraction of Elements (%)			
Sample Code	**Chemical formula**	**AMW (g/mol)**	**Density (g/cm^3)**	**Ag**	**O**	**B**	**Te**
G1	$10Ag_2O+58.5B_2O_3+31.5TeO_2$	114.174	4.914	0.189	0.348	0.111	0.352
G2	$15Ag_2O+55.25B_2O_3+29.75TeO_2$	120.705	4.923	0.268	0.318	0.099	0.314
G3	$20Ag_2O+52B_2O_3+28TeO_2$	127.236	4.965	0.339	0.292	0.088	0.281
G4	$25Ag_2O+48.75B_2O_3+26.25TeO_2$	133.767	5.082	0.403	0.268	0.079	0.25
G5	$30Ag_2O+42.25B_2O_3+22.75TeO_2$	135.243	5.248	0.479	0.239	0.068	0.215

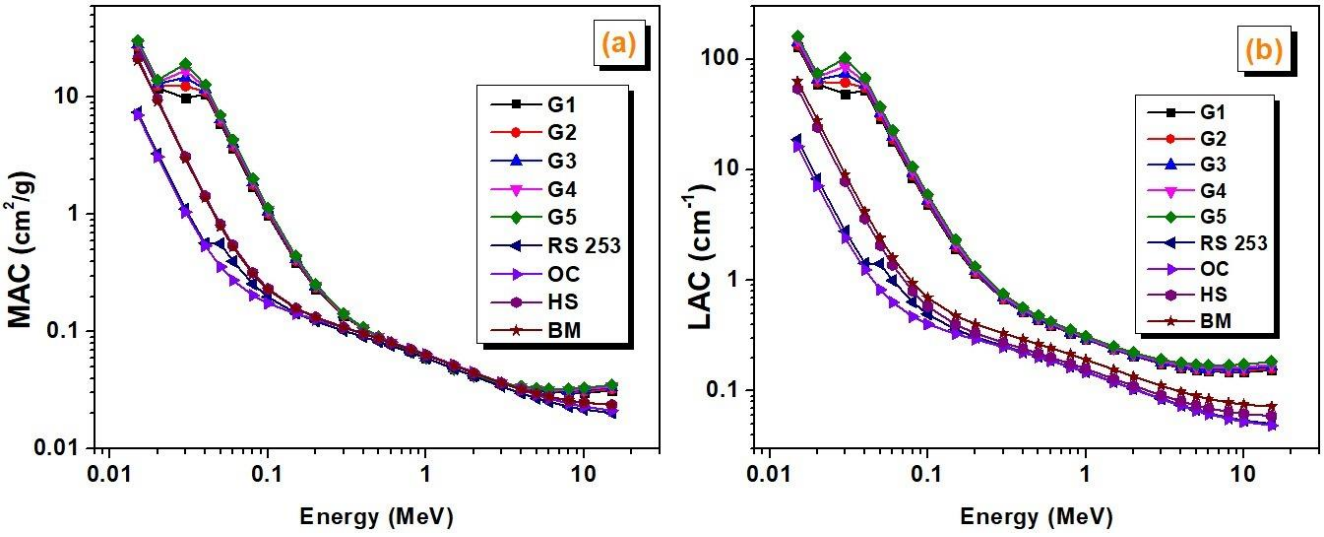

Figure 1. The variations of mass attenuation coefficients (a) and linear attenuation coefficients (b) versus incident photon energy.

In addition to the MAC values, the energy dependent variations of the LAC values are presented in Fig. 1 (b). Because the LAC parameters are obtained by multiplying the MAC parameters by density, the variations of LAC values are similar to the changes of MAC values as a function of photon energy. Furthermore, since this parameter is used to calculate other shielding parameters such as HVL and MFP, it is important to present a graphical variation. The densities of the materials compared that was used for comparison in this study were 2.5, 2.3, 2.5 and 3.05 for RS 253, OC, HS and BM, respectively. In

addition, the density values of the Ag tempered glasses examined ranged from 4.914 to 5.248. Considering these density values, greater differences were obtained in LAC values than MAC values for all samples examined with respect to each other.

Figs. 2 (a)-(b) shows the variation of HVL and MFP for Ag_2O doped boro-tellurite glass system as a function of incident photon energy. In a superior radiation shielding material, it is desirable that the material have lower MFP and HVL values. As shown in Figs. 2 (a)-(b), HVL and MFP values increase as a function of increasing energy. In the low energy zone, these values are close to zero. However, since most photons in the region where Compton scattering predominates tend to scatter and are therefore less likely to absorb, thicker materials are needed and photons have longer mean free paths. For the reason explained above, there is a sudden increase in HVL and MFP values in the middle energy region. As in MAC and LAC values, from Fig. 2, it can be seen that G5 sample has the best shielding characteristics among the examined samples. For example, in order to halve the number of photons at 15 MeV photon energy, the G5 sample should have a thickness of 3.75 cm, while the OC sample should have a thickness of 14.2 cm.

Table 2. Mass attenuation coefficients of the investigated materials in the energy range of 0.015-15 MeV.

Energy (MeV)	Mass attenuation coefficient (cm^2/g)								
	G1	**G2**	**G3**	**G4**	**G5**	**RS 253**	**OC**	**HS**	**BM**
1.50E-02	26.122	27.319	28.393	29.363	30.503	7.478	7.054	21.536	20.575
2.00E-02	12.045	12.589	13.078	13.519	14.037	3.312	3.105	9.660	9.208
3.00E-02	9.859	12.452	14.779	16.879	19.349	1.116	1.048	3.124	2.974
4.00E-02	10.627	11.203	11.719	12.185	12.734	0.569	0.541	1.442	1.376
5.00E-02	5.908	6.217	6.495	6.745	7.040	0.565	0.358	0.826	0.790
6.00E-02	3.652	3.836	4.002	4.151	4.327	0.399	0.275	0.547	0.526
8.00E-02	1.721	1.802	1.875	1.940	2.017	0.255	0.204	0.319	0.310
1.00E-01	0.981	1.024	1.062	1.096	1.136	0.198	0.175	0.233	0.228
1.50E-01	0.392	0.405	0.417	0.428	0.440	0.144	0.143	0.159	0.157
2.00E-01	0.233	0.238	0.243	0.248	0.253	0.123	0.127	0.133	0.132
3.00E-01	0.137	0.138	0.140	0.141	0.143	0.102	0.109	0.110	0.109
4.00E-01	0.105	0.106	0.107	0.107	0.108	0.090	0.097	0.096	0.096
5.00E-01	0.090	0.090	0.090	0.091	0.091	0.082	0.088	0.087	0.087
6.00E-01	0.080	0.080	0.080	0.080	0.081	0.076	0.081	0.081	0.080
8.00E-01	0.068	0.068	0.068	0.068	0.068	0.066	0.071	0.071	0.070
1.00E+00	0.060	0.060	0.060	0.060	0.060	0.060	0.064	0.063	0.063
1.50E+00	0.048	0.048	0.048	0.048	0.048	0.048	0.052	0.052	0.051
2.00E+00	0.042	0.042	0.042	0.042	0.042	0.042	0.045	0.045	0.044
3.00E+00	0.036	0.036	0.036	0.036	0.037	0.034	0.037	0.037	0.037
4.00E+00	0.033	0.033	0.034	0.034	0.034	0.030	0.032	0.032	0.032
5.00E+00	0.031	0.032	0.032	0.033	0.033	0.027	0.029	0.030	0.030
6.00E+00	0.031	0.031	0.032	0.032	0.032	0.025	0.027	0.028	0.028
8.00E+00	0.030	0.031	0.031	0.032	0.032	0.023	0.024	0.026	0.026
1.00E+01	0.030	0.031	0.032	0.032	0.033	0.022	0.023	0.025	0.025
1.50E+01	0.031	0.032	0.033	0.034	0.035	0.020	0.021	0.024	0.024

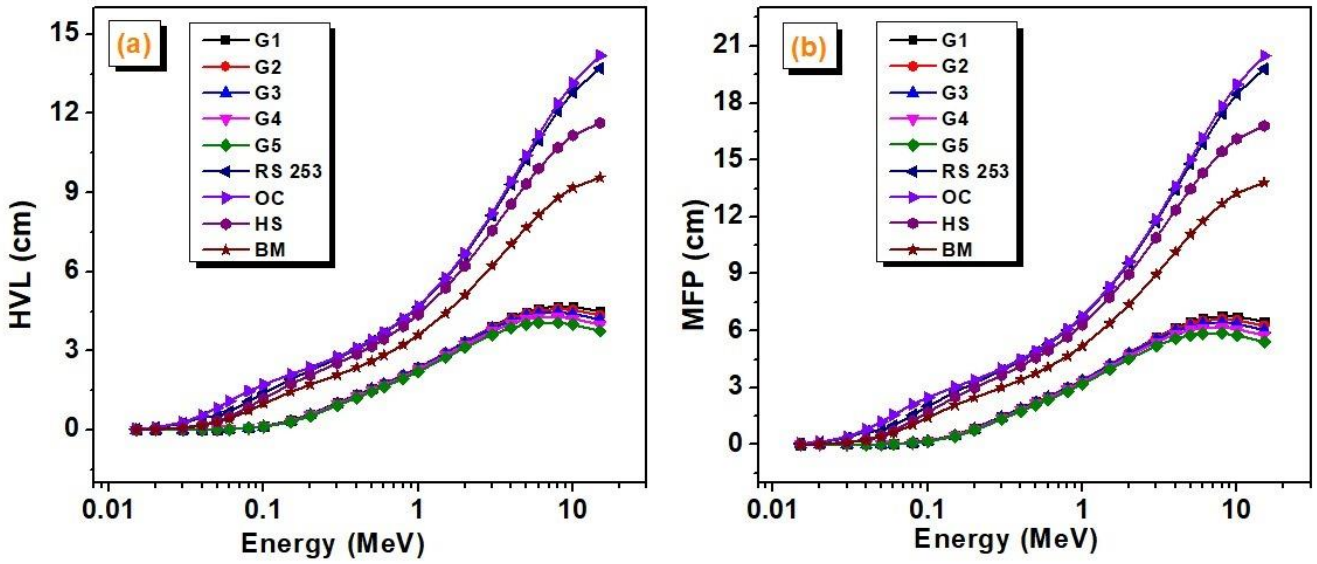

Figure 2. The changes of half-value layers (a) and mean free paths (b) versus incident photon energy.

On the other hand, atomic and electronic cross-section values of the sample investigated are presented in Figs. 3(a)-(b). The ACS and ECS gives the probability of interaction per atom and per electron in the unit volume of any material, respectively. If the numbers of atom and electron in the unit volume of material is high, the ACS and ECS values of the material will increase accordingly. Materials with high ACS and ECS values are considered to be better materials in terms of radiation shielding. In general, the ACS and ECS curves given in Figs. 3 (a)-(b) have similar variation. Unlike ECS values in the middle energy region (0.4-4 MeV), ACS values depend on the chemical composition of the material. Namely, while the ACS values are dependent on both chemical composition of material and incident photon energy in the whole energy region, ECS values are only dependent on photon energy in the energy region of 0.4-4 MeV. When all materials presented are evaluated together, it is seen that G5 sample has the highest ACS and ECS values and is OC sample has the lowest corresponding values. The ACS and ECS results obtained are in agreement with the previously described situation in the MAC, LAC, HVL and MFP values.

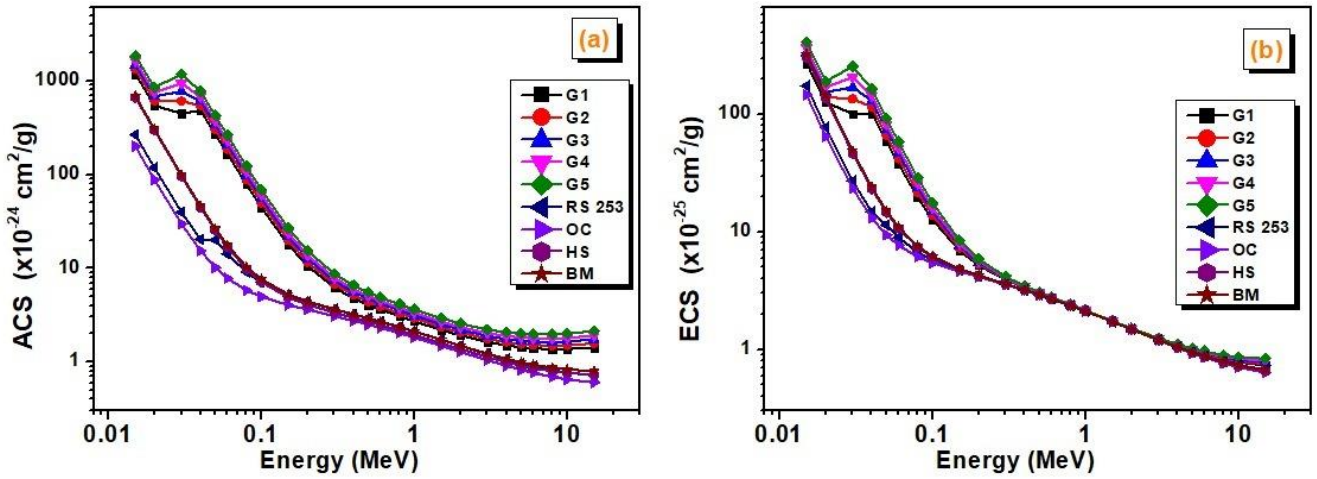

Figure 3. The changes of total atomic cross-section (a) and total electronic cross-section (b) as function of incident photon energy.

As with pure elements, there is a need for unique atomic and electron numbers that define a complex material containing more than one element at a given energy value. The unique number of atoms and electrons that characterize this complex material is called effective atomic and electron numbers, respectively. Additionally, knowing the energy-dependent values of these two parameters helps in material design that can be used in nuclear applications. The Z_{eff} values of the all present samples are given in Table 3 in order to make a satisfying assessment. The energy dependent variations of Z_{eff} and N_{eff} values are shown in Fig. 4 (a) and Fig. 4 (b), respectively. As shown in Fig. 4 (a) and Table 3, Z_{eff} values were higher in Ag_2O doped boro-tellurite glasses than in other materials. Especially in the energy region where the photoelectric effect is dominant, Z_{eff} values have maximum values. As a function of increasing energy, these values first sharply decrease in the low energy region, almost remains constant in the middle energy region and then slowly increase in the high energy region. In Ag_2O doped boro-tellurite glasses, the order of the Z_{eff} values in the all energy range is G5> G4> G3> G2> G1. Z_{eff} values obtained also support that G5 has the best shielding capacity. This ordering is proof that the radiation protection performances of present glasses increase with increasing of molar percentage of Ag_2O compound contained of telluride glasses.

Table 3. Effective atomic numbers of the investigated materials in the energy range 0.015-15 MeV.

Energy (MeV)	Effective atomic numbers (Z_{eff})								
	G1	**G2**	**G3**	**G4**	**G5**	**RS 253**	**OC**	**HS**	**BM**
1.50E-02	43.897	44.223	44.496	44.727	44.984	15.354	13.789	21.911	21.376
2.00E-02	43.541	43.910	44.220	44.484	44.776	15.316	13.585	21.767	21.283
3.00E-02	44.444	45.116	45.528	45.806	46.059	14.729	12.754	20.806	20.489
4.00E-02	47.415	47.312	47.228	47.159	47.084	13.794	11.730	19.223	19.130
5.00E-02	45.993	46.087	46.163	46.227	46.297	17.619	10.849	17.419	17.548
6.00E-02	44.183	44.507	44.777	45.004	45.253	15.972	10.207	15.730	16.042
8.00E-02	39.793	40.591	41.273	41.863	42.527	13.603	9.469	13.205	13.748
1.00E-01	35.120	36.291	37.322	38.238	39.297	12.264	9.121	11.713	12.369
1.50E-01	25.714	27.203	28.600	29.915	31.531	10.900	8.810	10.161	10.917
2.00E-01	20.365	21.765	23.129	24.459	26.158	10.462	8.718	9.668	10.452
3.00E-01	15.892	17.060	18.235	19.416	20.982	10.187	8.662	9.361	10.162
4.00E-01	14.316	15.367	16.435	17.523	18.984	10.103	8.644	9.269	10.075
5.00E-01	13.618	14.610	15.626	16.664	18.067	10.068	8.637	9.231	10.038
6.00E-01	13.255	14.216	15.202	16.213	17.584	10.050	8.633	9.211	10.019
8.00E-01	12.901	13.830	14.786	15.769	17.106	10.033	8.629	9.191	10.001
1.00E+00	12.735	13.649	14.591	15.560	16.880	10.024	8.627	9.182	9.991
1.50E+00	12.646	13.553	14.488	15.451	16.764	10.022	8.630	9.186	9.996
2.00E+00	12.802	13.729	14.681	15.661	16.994	10.036	8.648	9.232	10.038
3.00E+00	13.373	14.363	15.376	16.412	17.814	10.087	8.709	9.383	10.177
4.00E+00	14.041	15.102	16.181	17.278	18.752	10.148	8.783	9.566	10.345
5.00E+00	14.719	15.847	16.987	18.141	19.678	10.210	8.860	9.757	10.520
6.00E+00	15.364	16.552	17.746	18.948	20.538	10.272	8.939	9.948	10.694
8.00E+00	16.548	17.836	19.119	20.395	22.065	10.388	9.088	10.310	11.018
1.00E+01	17.571	18.936	20.282	21.611	23.331	10.490	9.222	10.632	11.305
1.50E+01	19.515	20.997	22.436	23.832	25.608	10.688	9.488	11.266	11.859

Effective electron density (or effective electron number ; N_{eff}) represents the average number of electrons per unit mass, depending on the photon energy of the material interacting with the photons.

Therefore, its unit is electrons/g. The effective electron density are directly related to MAC and ECS values. N_{eff} is the most important parameter that indicates the effective conductivity of a material at a given ambient temperature depending on the excitatory photon energy. In this study, the effective electron density were calculated with help of MAC and ECS values and the results obtained are graphically presented in Fig. 4(b). As can be seen from this figure, the variations of N_{eff} results obtained as a function of incident photon energy are similar with the changes of Z_{eff} values. However, the N_{eff} values in the low energy region where is predominat of photoelectric effect are more dependent on chemical composition of materials with respect to Z_{eff} values. On the contrary, it was observed that this situation is reversed with increasing photon energy (especiall high energy region where pair production predominates). Furthermore, it is clearly seen from Figs. 4(a) and (b) that there are jumps at about 0.04 MeV. These jumps can be attributed by *K*-shell absoption edges (about 0.032 MeV for Te and about 0.026 MeV for Ag) of Te and Ag elements that are contain in boro telluride ternary glasses. In addition, it was observed that the N_{eff} values of the investigated glasses is G1> G2> G3> G4> G5 contrary to the order observed in the Z_{eff} values.

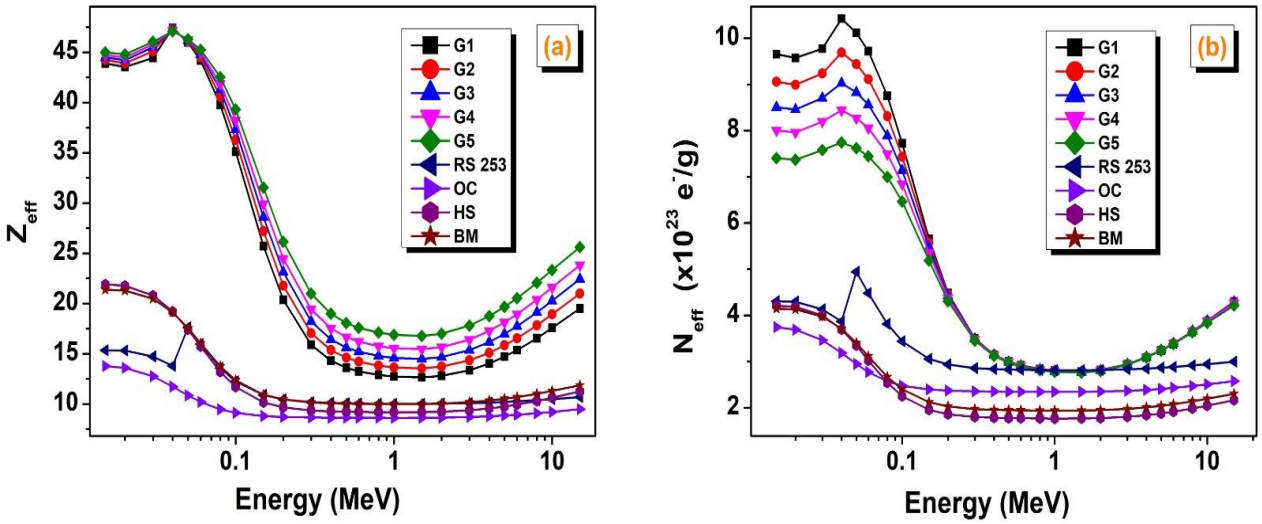

Figure 4. The variations of effective atomic number (a) and effective electron density (b) as function of incident photon energy.

Another important parameter in photon matter interactions is effective conductivity (σ_{eff}). This parameter is related to how much free electrons are formed in the unit volume of material with interacted photon energy. This parameter is directly proportional to the physical density of the material, the effective electron density, and the temperature of the environment in which the interaction occurs. Therefore, variations in σ_{eff} values related to photon energy and N_{eff} values are shown in Fig. 5 (a) and Fig. 5 (b), respectively. From Fig. 5(a), it is seen that the formation of free electrons in the region dominated by photoelectric absorption is higher than in other regions. Because the photons in this region have low energies and higher wavelengths, they are more likely to interact with target material electrons. This high probability leads to more photon absorption by electrons, resulting in more free electrons. The G1 sample had the highest N_{eff} value as previously mentioned and the highest σ_{eff} value was obtained in this sample. The σ_{eff} values of all Ag_2O doped glasses are considerably higher than other comparative materials. In the energy regions where Compton scattering and pair production are dominant, the σ_{eff} values of Ag_2O doped glasses are almost independent of the chemical composition of the materials. Because of the high penetration of the photons in these regions, the probabilities of interaction with the target material electrons is lower than in the lower photon energy region. Furthermore, it can also be

seen from Fig. 5 (a) that the σ_{eff} values in RS 253, BM and OC samples are smaller than boro telluride glasses under examination. The variations of effective electron density versus N_{eff} values are presented in Fig. 5 (b). From this graph, it is seen that the highest σ_{eff} and N_{eff} change is in Ag_2O doped glasses. In RS 253, BM and OC samples, this change is considerably smaller than in other samples. Because the absorption capacity of these materials, namely, the probabilities of interaction with the incoming photon is quite low.

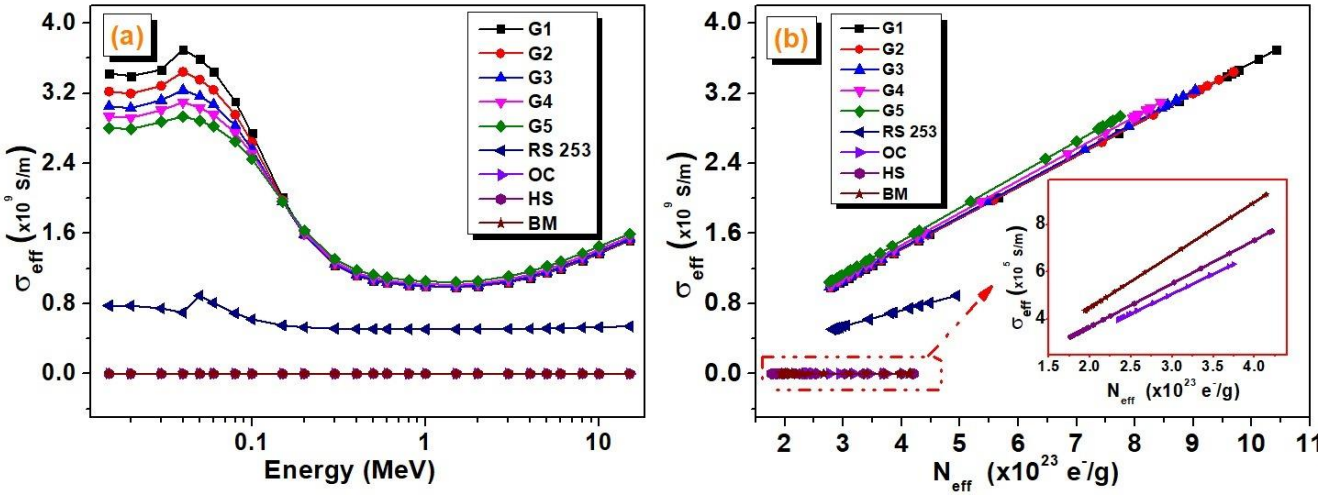

Figure 5. (a) The variations of effective conductivity versus photon energy and (b) The changes of effective conductivity versus effective electron density.

CONCLUSION

In this study, radiation shielding parameters of Ag_2O doped boro-tellurite glasses were presented to determine of photon protection features. The calculations presented in the study were performed using Phy-X / PSD software. The MAC, LAC, HVL, MFP, ACS, ECS, Z_{eff}, N_{eff} and σ_{eff} changes of the present samples were presented in the energy range of 0.015-15 MeV. In order to make a satisfactory evaluation, the results were compared with RS 253 glass and OC, BM and HS concretes. As a result of the study, it was found that Ag_2O doped glasses had a very high probabilities of interacting with photon compared to other comparative materials. This demonstrates the usefulness of Ag_2O doped boro-tellurite glasses in applications requiring radiation safety. It was observed that the absorption capacity increased with increasing Ag_2O concentration for the examined glasses. The best radiation absorption capacity was observed in the 30% Ag_2O doped boro-telluride glass.

REFERENCES

Abdalsalam AH, Sayyed M, Hussein TA, Şakar E, Mhareb M, Şakar BC, Alim B, Kaky KM. 2019. A study of gamma attenuation property of UHMWPE/Bi2O3 nanocomposites. Chemical Physics, 523: 92-98.

Agar O, Sayyed MI, Akman E, Tekin HO, Kacal MR, 2019. An extensive investigation on gamma ray shielding features of Pd/Ag-based alloys. Nuclear Engineering Technology, 51: 853-859.

Ahmad MM, Yousef ES, Moustafa ES. 2006. Dielectric properties of the ternary $TeO_2/Nb_2O_5/ZnO$ glasses. Physica B: Condensed Matter, 371(1):74-80.

Akman F, Khattari ZY, Kaçal MR, Sayyed MI, Afaneh F, 2019. The radiation shielding features for some silicide, boride and oxide types ceramics. Radiation Physics and Chemistry, 160: 9-14.

Akman F, Kaçal MR, Sayyed MI, Karataş HA, 2019. Study of gamma radiation attenuation properties of some selected ternary alloys. Journal of Alloys and Compounds, 782: 315-322.

Alım, B, Şakar, E, Baltakesmez A, Han İ, Sayyed, M, Demir L, 2020. Experimental investigation of radiation shielding performances of some important AISI-coded stainless steels: Part I. Radiation Physics and Chemistry, 166: 108455.

Alım B, Şakar E, Han İ, Sayyed M, 2020b. Evaluation the gamma, charged particle and fast neutron shielding performances of some important AISI-coded stainless steels Part II. Radiation Physics and Chemistry, 166: 108454.

Aygün B, Şakar E, Korkut T, Sayyed MI, Karabulut A, 2019. New high temperature resistant heavy concretes for fast neutron and gamma radiation shielding. Radiochimica Acta, 107(4): 359–367.

Bashter II. 1997. Calculation of radiation attenuation coefficients for shielding concretes. Annals of Nuclear Energy 24 (17): 1389-1401.

Desirena H, Schülzgen A, Sabet S, Ramos-Ortiz G, de la Rosa E, Peyghambarian N. 2009. Effect of alkali metal oxides R_2O (R = Li, Na, K, Rb and Cs) and network intermediate MO (M = Zn, Mg, Ba and Pb) in tellurite glasses. Optical Materials, 31 (6): 784-789.

El-Mallawany R, Saunders GA. 1988. Elastic Properties of Binary, Ternary and Quaternary Rare-Earth Tellurite Glasses. Journal of Material Science Letters, 7 (8): 870-874.

El-Mallawany R, Sidkey M, Khafagy A, Afifi H. 1994. Ultrasonic attenuation of tellurite glasses. Materials Chemistry and Physics, 37 (2): 197-200.

El-Mallawany R. 1992. The optical properties of tellurite glasses. Journal of Applied Physics, 72 (5): 1774-1777.

El-Mallawany R. 2016. Tellurite glasses handbook: Physical properties and data: Second edition.

El-Moneim AA. 2009. Tellurite glasses: Correlations between elastic moduli and compositional parameters, Physics and Chemistry of Glasses: European Journal of Glass Science and Technology Part B, 50: 407-417.

Ersundu AE, Büyükyıldız M, Çelikbilek Ersundu M, Şakar E, Kurudirek M. 2018. The heavy metal oxide glasses within the WO_3-MoO_3-TeO_2 system to investigate the shielding properties of radiation applications. Progress in Nuclear Energy, 104: 280-287.

Gerward L, Guilbert N, Jensen KB, Levring H. 2004. WinXCom - a program for calculating X-ray attenuation coefficients. Radiation Physics and Chemistry 71 (3): 653-654.

Halimah MK, Daud WM, Sidek HAA, Zainal AT, Zainul H, Hassan J. 2005. Optical properties of borotellurite glasses. American Journal of Applied Sciences, 63-66.

Han I, Un A, Alim B, 2015. Investigation of Comet Wild-2 in terms of effective atomic numbers. Advance in Space Research, 56 (10): 2275-2287.

Han I, Demir L, 2010. Studies on effective atomic numbers, electron densities and mass attenuation coefficients in Au alloys. Journal of X-ray Science and Technology, 18(1): 39-46.

Han I, Aygun M, Demir L, Sahin Y, 2012. Determination of effective atomic numbers for 3d transition metal alloys with a new semi-empirical approach. Annals of Nuclear energy, 39: 56-61.

Han I, Demir L, 2009. Studies on effective atomic numbers, electron densities from mass attenuation coefficients in TixCo1-x and CoxCu1-x alloys. Nuclear Instruments and Methods in Physics Research B, 267: 3505-3510.

Lakshminarayana G, Baki SO, Lira A, Sayyed MI, Kityk IV, Halimah MK, Mahdi MA. 2017. X-ray photoelectron spectroscopy (XPS) and radiation shielding parameters investigations for zinc molybdenum borotellurite glasses containing different network modifiers. Journal of Materials Science, 52 (12): 7394-7414.

Lakshminarayana G, Kumar A, Dong MG, Sayyed MI, Long NV, Mahdi MA. 2018. Exploration of gamma radiation shielding features for titanate bismuth borotellurite glasses using relevant software program and Monte Carlo simulation code. Journal of Non-Crystalline Solids, 481: 65-73.

Lambson EF, Saunders GA, Bridge B, El-Mallawany R. 1984. The elastic behaviour of TeO_2 glass under uniaxial and hydrostatic pressure. Journal of Non-Crystalline Solids, 69 (1): 117-133.

Öveçoğlu ML, Özen G, Cenk S. 2006. Microstructural characterization and crystallization behavior of $(1-x)TeO_2–xWO_3$ (x = 0.15, 0.25, 0.3 mol) glasses, Journal of the European Ceramic Society, 26 (7): 1149-1158.

Rajendran V, Palanivelu N, Chaudhuri BK, Goswami K. 2003. Characterization of semiconducting V_2O_5-Bi_2O_3-TeO_2 glasses through ultrasonic measurements. Journal of Non-Crystalline Solids, 320 (1-3): 195-209.

Sakar, E, Buyukyildiz M, Alim B, Sakar BC, Kurudirek M, 2019. Leaded brass alloys for gamma-ray shielding applications. Radiation Physcis Chemistry 159: 64-69.

Sayyed MI, Elhouichet H. 2017. Variation of energy absorption and exposure buildup factors with incident photon energy and penetration depth for boro-tellurite (B_2O_3-TeO_2) glasses. Radiation Physics and Chemistry, 130: 335-342.

Shioya K, Komatsu T, Kim HG, Sato R, Matusita R. 1995. Optical properties of transparent glass-ceramics in K_2O-Nb_2O_5-TeO_2 glasses. Journal of Non-Crystalline Solids, 189 (1-2): 16-24.

Sidkey MA, El-Mallawany R, Nakhla RI, Abd El-Moneim A. 1997. Ultrasonic studies of $(TeO_2)1-x-(V_2O_5)x$ glasses. Journal of Non-Crystalline Solids, 215 (1): 75-82.

Stanworth JE. 1952. Tellurite Glasses. Nature, 169: 581-582.

Şakar E, Özpolat ÖF, Alım B, Sayyed MI, Kurudirek M. 2020. Phy-X / PSD: Development of a user friendly online software for calculation of parameters relevant to radiation shielding and dosimetry, Radiation Physics and Chemistry, 166: 108496.

Xu S, Wang P, Zheng R, Wei W, Peng B. 2013. Effects of alkaline-earth fluorides and OH^- on spectroscopic properties of Yb^{3+} doped $TeO_2–ZnO–B_2O_3$ based glasses. Journal of Luminescence 140: 26-29.